Chinese Physics B

TOPICAL REVIEW

Exploring Majorana zero modes in iron-based superconductors

To cite this article: Geng Li *et al* 2022 *Chinese Phys. B* **31** 080301

TOPICAL REVIEW — Celebrating 30 Years of *Chinese Physics B*

Exploring Majorana zero modes in iron-based superconductors

Geng Li(李更)[1,2,3], Shiyu Zhu(朱诗雨)[1,2], Peng Fan(范朋)[1,2], Lu Cao(曹路)[1,2], and Hong-Jun Gao(高鸿钧)[1,2,3,†]

[1] *Institute of Physics, Chinese Academy of Sciences, Beijing* 100190, *China*
[2] *School of Physical Sciences, University of Chinese Academy of Sciences, Beijing* 100190, *China*
[3] *Songshan Lake Materials Laboratory, Dongguan* 523808, *China*

(Received 7 April 2022; revised manuscript received 17 May 2022; accepted manuscript online 18 May 2022)

Majorana zero modes (MZMs) are Majorana-fermion-like quasiparticles existing in crystals or hybrid platforms with topologically non-trivial electronic structures. They obey non-Abelian braiding statistics and are considered promising to realize topological quantum computing. Discovery of MZM in the vortices of the iron-based superconductors (IBSs) has recently fueled the Majorana research in a way which not only removes the material barrier requiring construction of complicated hybrid artificial structures, but also enables observation of pure MZMs under higher temperatures. So far, MZMs have been observed in iron-based superconductors including $FeTe_{0.55}Se_{0.45}$, $(Li_{0.84}Fe_{0.16})OHFeSe$, $CaKFe_4As_4$, and LiFeAs. In this topical review, we present an overview of the recent STM studies on the MZMs in IBSs. We start with the observation of MZMs in the vortices in $FeTe_{0.55}Se_{0.45}$ and discuss the pros and cons of $FeTe_{0.55}Se_{0.45}$ compared with other platforms. We then review the following up discovery of MZMs in vortices of $CaKFe_4As_4$, impurity-assisted vortices of LiFeAs, and quantum anomalous vortices in $FeTe_{0.55}Se_{0.45}$, illustrating the pathway of the developments of MZM research in IBSs. Finally, we give perspective on future experimental works in this field.

Keywords: Majorana zero mode, iron-based superconductors, topological surface states, scanning tunneling microscopy

PACS: 03.75.Lm, 74.25.–q, 74.70.–b

DOI: 10.1088/1674-1056/ac70c3

1. Introduction

The search for Majorana fermion dates back to the 1937 theoretical proposal of Ettore Majorana, an Italian physicist, by predicting a unique fermionic particle whose antiparticle is itself.[1] While the predicted Majorana fermions never show up as free particles, condensed matter theorists have found an alternative by constructing neutrally-charged quasiparticle excitations with particle and anti-particle symmetry, which are now referred to as Majorana excitations or Majorana zero modes.[2–4] MZMs appear in pairs that could be distant in real space. As a result, MZMs are immune to local perturbations and their non-Abelian statistical nature allows fault-tolerant quantum computation.[5–8] This fascinating property sparks people's passion into the Majorana research and tons of material platforms have been theoretically proposed in the past two to three decades, leading to a fast boost in the field.[9–19]

Following these predictions, several platforms have been realized by the experimentalists. Large spin–orbital coupling (SOC) semiconducting nanowire,[20–24] 1D magnetic atomic chain,[25–30] 2D magnetic islands,[31–35] and 3D topological insulator,[36,37] in proximity to traditional s-wave superconductors, have been demonstrated as platforms supporting MZMs. These platforms require fabricating of complicated hybrid artificial structures and thus additional caution has been taken to differentiate the artefacts and/or noise of, e.g., the interface disorders from the real signal.[20] Also, extremely low temperatures are needed in observing the MZMs.

The observations of topological surface state (TSS) by angle-resolved photoemission spectroscopy (ARPES)[38] and zero-bias peak (ZBP) in the vortices by scanning tunneling microscopy/spectroscopy (STM/S)[39] in $FeTe_{0.55}Se_{0.45}$ open up a new platform hosting MZMs, i.e., the iron-based superconductors.[40,41] The IBSs can be treated as a self-hybrid system that has conventional superconductivity in bulk and topological superconductivity on the surface. Once the IBSs are cooled down below T_c, the topological surface states become superconducting due to the proximity effect. As a result, the topological superconductivity can be realized on the surfaces of IBSs, which are single materials without necessity to construct additional hybrid structures. The following up experiments performed in $(Li_{0.84}Fe_{0.16})OHFeSe$,[42] $CaKFe_4As_4$,[43] and LiFeAs[44] further demonstrate that IBSs emerge as a big family feasible for Majorana research.[45–48] Compared with the former platforms mainly achieved by hybrid structures, IBSs possess the advantages of single material and higher surviving temperature (due to their high-T_c superconducting nature) for MZMs. The simple material structure and the existence of pure MZM make IBSs ideal platforms for MZM research.[41]

In this review, we will focus on recent STM/S studies on MZMs in IBSs. We start with $FeTe_{0.55}Se_{0.45}$ in Section 2 where we review the MZMs in the vortices, quantized

†Corresponding author. E-mail: hjgao@iphy.ac.cn

sequence of MZM and Caroli–de Gennes–Matricon bound states (CBSs),[49,50] and the nearly quantized conductance of the MZMs. Then we review the MZMs in two other IBSs $CaKFe_4As_4$ and LiFeAs and discuss their own advantages. In Section 5 we review a special case for MZM where the external magnetic field is not necessary. The introduction of different MZM platforms in IBSs is followed by a section describing possible control over their topological band structures by utilizing uniaxial strain in LiFeAs. We summarize the review with a perspective on future directions in Majorana research by STM/S.

2. Discovery of Majorana zero mode in $FeTe_{0.55}Se_{0.45}$

2.1. Evidence for MZM in $FeTe_{0.55}Se_{0.45}$

Benefiting from the ARPES and theoretical efforts,[38,51–54] the iron-based superconductor Fe(Te, Se) is supported to host topological non-trivial surface Dirac bands, making it a topological superconducting material. According to the Fu–Kane model,[9] the MZMs are expected to appear in the vortex cores, due to the superconductivity proximity effect in TSS. Wang *et al.* discovered MZM in $FeTe_{0.55}Se_{0.45}$ by STM/S.[39] The topographic image shows the square lattice with clearly resolved Te (brighter) and Se (darker) atoms on the cleaved crystal surface (Fig. 1(a)), indicating the intrinsic inhomogeneity of local Te/Se distribution. When an external magnetic field is applied, the vortices emerge in the $\mathrm{d}I/\mathrm{d}V$ map at zero energy (Fig. 1(b)), implying existence of in-gap vortex bound states.

The existence of MZM is strongly supported by $\mathrm{d}I/\mathrm{d}V$ linecuts through the vortex cores. A sharp and robust ZBP (Fig. 1(c)) shows up along the linecut across the vortex in Fig. 1(b). Unlike the spatially dispersion CBSs, the ZBP does not split or shift when moving away the vortex center, providing an important piece of evidence of pure MZMs in the vortex cores. This conclusion is further supported by comparison with ARPES results (Fig. 1(d)) and theoretical calculation (Fig. 1(e)). The existence of MZMs in Fe(Te, Se) material has also been reported by other independent works.[48]

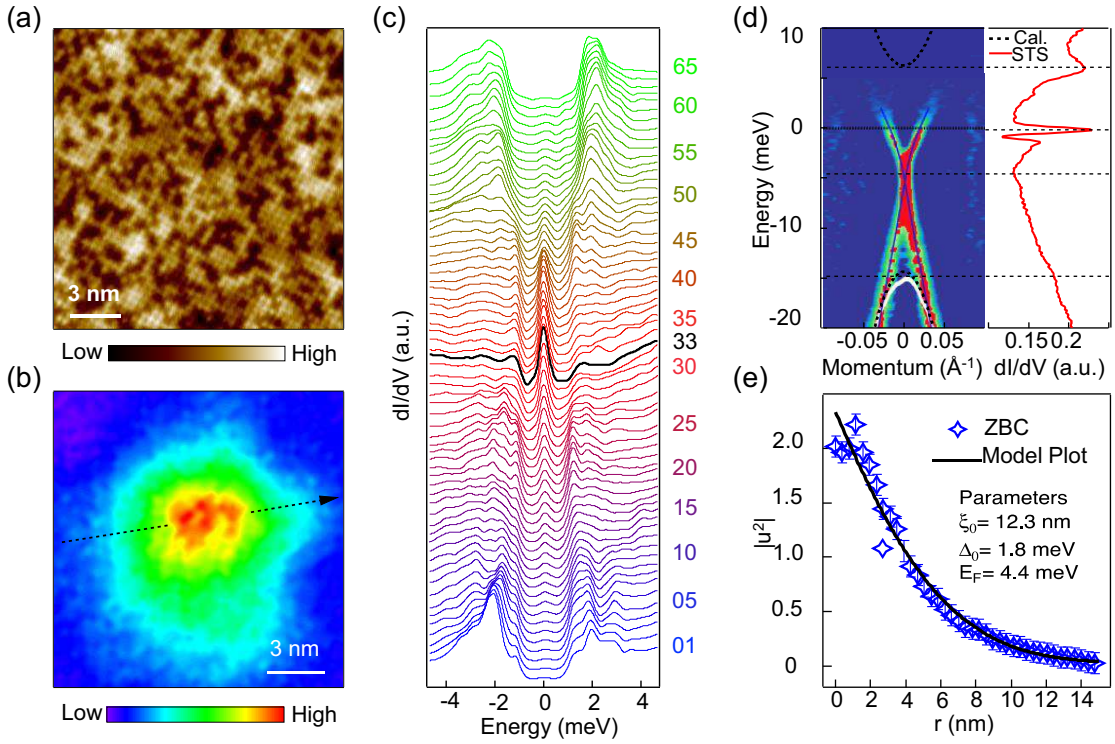

Fig. 1. MZMs in the vortex core of $FeTe_{0.55}Se_{0.45}$. (a) STM topography of $FeTe_{0.55}Se_{0.45}$. (b) A zero-bias conductance map around a vortex core. (c) A line-cut intensity plot along the black dashed line in (b). (d) Comparison between the ARPES and the STS results. (e) Comparison between the measured ZBP peak intensity as a function of distance and a theoretical calculation of the MZM spatial profile.[39]

2.2. Half-integer level shift of vortex bound states in $FeTe_{0.55}Se_{0.45}$

One mystery with the $FeTe_{0.55}Se_{0.45}$ system is that only a small fraction of the vortices hosts MZMs. Wang *et al.* found the ratio of the vortices with MZMs is $\sim 20\%$.[39] Machida *et al.* further showed that this value decreased with increasing magnetic field.[48,55] The reason behind was revealed by a systemic and detailed STM study in $FeTe_{0.55}Se_{0.45}$ by Kong *et al.*[56] In an external magnetic field, two classes of vortices appear on $FeTe_{0.55}Se_{0.45}$ surface, named as topological vortices (with MZMs) and ordinary vortices (without MZMs). Besides the existence of MZMs, a set of higher-energy vortex bound states are also in play.

Figures 2(a) and 2(b) show the typical cases of a topo-

logical vortex and an ordinary vortex. Benefiting from the large Δ^2/E_F value in Fe(Te, Se), the MZM and CBS peaks are widely separated with each other, driving the system under the quantum limit. For the topological vortex with MZM, the energy levels of the vortex bound states show a quantized sequence of 0:1:2:3. For the ordinary vortex without MZM, the sequence is 0.5:1.5:2.5:3.5, taking a half-integer level shift with the topological one. The statistics of 35 topological vortices and 26 ordinary vortices reproduce the quantized sequence of energy distribution, confirming the half-integer level shift related with the presence/absence of MZMs between two classes of vortices. This half-integer level shift is raised from the spin locking of topological Dirac surface state, which provides an additional 1/2 to the angular momentum (eigenstates) of vortex bound states when compared with that from bulk bands. This scenario explains the topological nature of MZMs in $FeTe_{0.55}Se_{0.45}$.[56] It also draws people's attention to the low yield and unpredictable topological vortices caused by the intrinsic inhomogeneity of $FeTe_{0.55}Se_{0.45}$.

2.3. Nearly quantized conductance plateau of MZM in $FeTe_{0.55}Se_{0.45}$

While non-split ZBPs and integer quantized vortex bound states are indeed characters of plausible MZMs, more direct evidences are still needed to confirm the existence of MZMs.[57–59] A stronger evidence for MZM is the resonant Andreev reflection protected by the inherent Majorana particle–hole symmetry, which has been theoretically proposed to show a quantized conductance plateau in ideal conditions.[7,60–63]

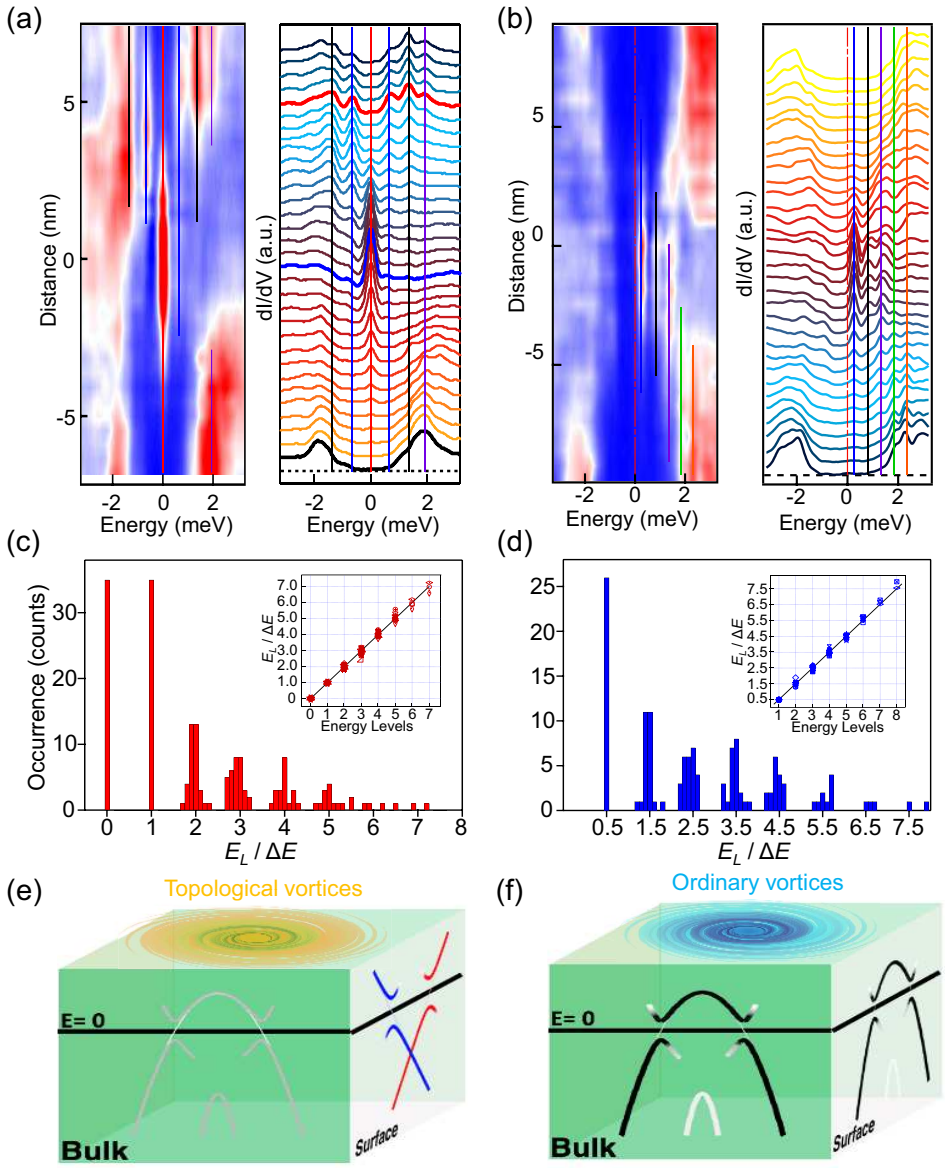

Fig. 2. Two classes of vortices in $FeTe_{0.55}Se_{0.45}$. (a) The intensity plot (left panel) and waterfall plot (right panel) of a dI/dV linecut through a topological vortex core, presenting the integer quantized vortex bond states. (b) The intensity plot (left panel) and waterfall plot (right panel) of a dI/dV linecut through an ordinary vortex core, presenting the half-odd-integer quantized CBSs. (c) A histogram of averaged level energies for 35 topological vortices. (d) A histogram of averaged level energies for 26 ordinary vortices. (e) Schematic plot of the underlying topological non-trivial Dirac surface bands of a topological vortex. (f) Schematic plot of the underlying topological trivial bands of an ordinary vortex.[56]

In 2020, Zhu *et al.* reported the nearly quantized Majorana conductance plateau in tunnel-coupling dependent measurements by varying the STM tunnel-barrier conductance G_N (Fig. 3(a)).[45] When preforming the tunnel-coupling dependent measurement, the ZBP remains a well-defined peak firmly located at zero energy. The absolute conductance of spectra keeps increasing expect that saturates at zero energy (Fig. 3(b)). The saturation of conductance shows a plateau feature when expanding the spectra in G_N dimension in a 3D plot (Fig. 3(c)). In this typical case in Fig. 3(c), the zero-energy conductance curve shows an average conductance of 0.64 G_0 (Fig. 3(d)), where G_0 is the quantized conductance $2e^2/h$. In striking contrast, all the non-zero-energy conductances show monotonic increasing features (Fig. 3(e)). The statistic of 31 measurements shows the nearly quantized value of conductance with one of them reaching the quantized conductance (Figs. 3(f) and 3(g)), providing quantitative evidence for the existence of Majorana modes.[64]

2.4. Further efforts for Majorana modes

The series of works on Fe(Te, Se) confirm the existence of MZMs in the vortices. Thanks to the high T_c and large Δ^2/E_F value, the iron-based superconductors holding pure MZMs are considered to be 'Goldilocks' materials.[65] However, more experimental and theoretical efforts are still needed towards realization of Majorana braiding and topological quantum qubits. After the confirmation and understanding of MZMs in vortices, the controllability and tunability will be the next topic for physicists. In order to obtain controllable MZMs, higher ratio of the topological vortices is the first challenge. As discussed above, both the distribution of two classes of vortices and the various plateau conductance values indicate strong inhomogeneous in Fe(Te, Se), setting obstacles to its potential application. For example, by performing a statistical analysis

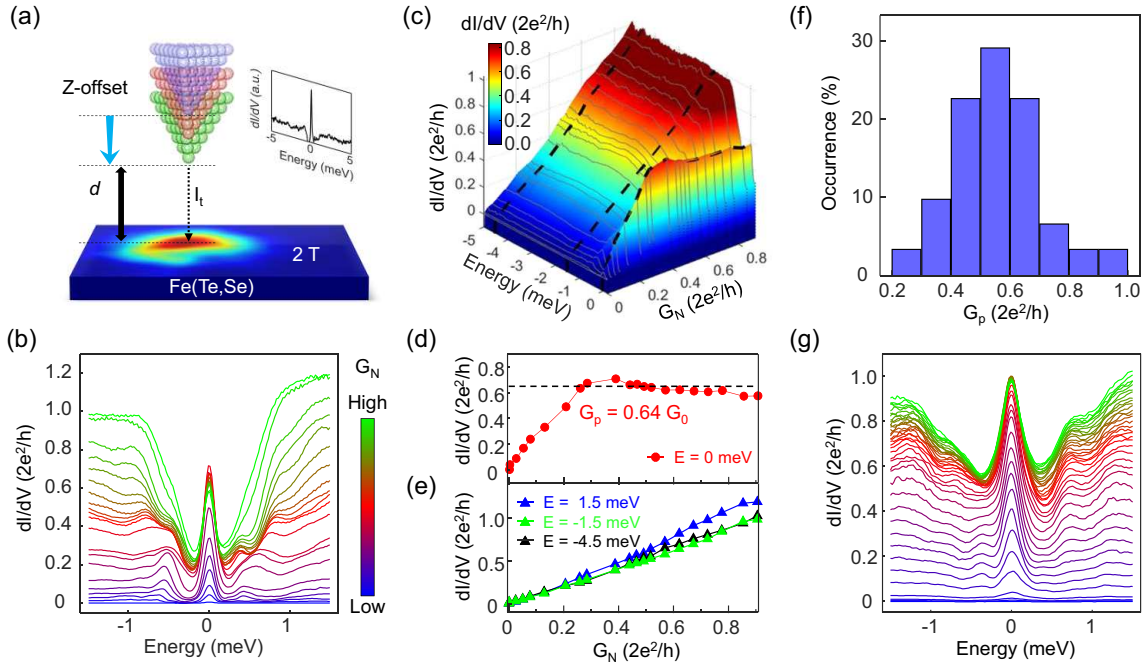

Fig. 3. Nearly-quantized Majorana conductance plateau in $FeTe_{0.55}Se_{0.45}$. (a) A schematic of variable tunnel coupling STM/S method. Larger tunnel coupling corresponds to smaller d and larger tunneling-barrier conductance (G_N). (b) An overlapping plot of dI/dV spectra under different tunnel coupling values parameterized in G_N. (c) A three-dimensional plot of tunnel coupling dependent measurement, dI/dV (E, G_N). (d) The zero-energy conductance curve from (b) and (c), showing a plateau behavior with the plateau conductance (G_p) equal to (0.64 ± 0.04) G_0. (e) Three high-energy conductance curves, showing monotonically increasing behavior with G_N. (f) A histogram of the G_p from 31 sets of data. (g) The overlapping plot of 38 dI/dV spectra selected from a topological vortex that reaches a quantized conductance plateau.[45]

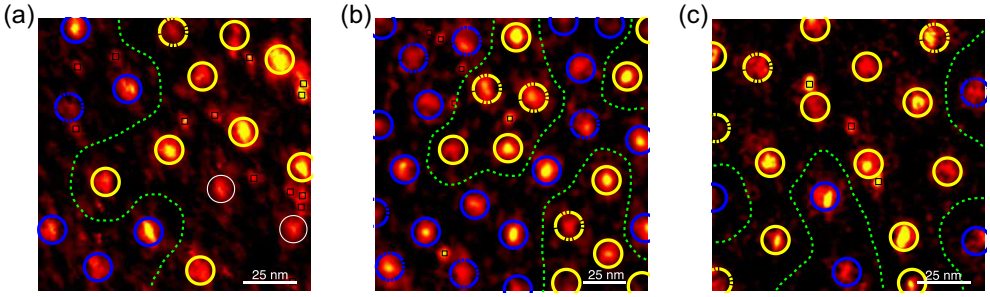

Fig. 4. Spatial distribution of the two classes of vortices. (a)–(c) The zero-bias conductance maps of three well-separated regions. The yellow circles mark topological vortices with MZMs and the blue circles mark ordinary vortices without MZMs. The green dashed lines encircle the same class of vortices. Topological vortices and ordinary vortices usually group together, which indicates that topological region and trivial region coexist in the sample surface due to spatial inhomogeneity.[56]

of the topological nature of vortices in Fe(Te, Se), Kong *et al.* observed that the topological and ordinary vortices both exist in the same field of view (Fig. 4) and that vortices that belong to the same class usually group together.[56] The reason behind was attributed to the inhomogeneous electronic structure of Fe(Te, Se) induced by Te doping. To obtain higher topological vortex ratio, increasing the material quality or looking for better platforms are both feasible solutions.

3. MZM in $CaKFe_4As_4$

The iron-chalcogenide superconductors have large superconducting (SC) gap, small Fermi energy, and nontrivial band structure in a single material.[39,42] These advantages permit them as good Majorana-hosting materials. However, the strong inhomogeneity may impede the application of iron-chalcogenide superconductors.[48,56,66] In the effort of exploring other platforms of MZM, the iron-pnictide superconductors have come to the top of the list.

Several types of iron-pnictides superconductors have been demonstrated to have topological nontrivial Dirac surface states.[52] In the STM experiments, MZM is discovered in the vortices. Liu *et al.* have identified Dirac surface states and MZM in $CaKFe_4As_4$ for the first time.[43] Meanwhile, the multiple vortex bound states with integer-quantization sequences can be accurately reproduced by the model calculation.

$CaKFe_4As_4$ can be viewed as $CaFe_2As_2$ and KFe_2As_2 intercalating with each other (Fig. 5(a)).[67] This special structure induces high-T_c superconductivity[68] and breaks the glide-mirror symmetry along the c-axis due to inequivalence of the Ca and K atoms. The glide-mirror symmetry breaking in $CaKFe_4As_4$ gives rise to a topological band inversion with a SOC gap of 20–30 meV near E_F, as shown in Fig. 5(b). The calculated results have been confirmed by ARPES experiments in Fig. 5(c). The Dirac surface band around Γ is directly observed by ARPES in Figs. 5(d)–5(g). In the undoped $CaKFe_4As_4$, the ARPES spectral intensity plots (Fig. 5(d)) and its second derivation (Fig. 5(f)) within the red box in Fig. 5(d) show the linear-like dispersion around E_F. In the K-doped sample, the Dirac surface band is directly observed (Figs. 5(e) and 5(g)).

After cooling down the sample below T_c, the STM experiments were performed to explore the MZM. The cleaved surface of $CaKFe_4As_4$ is formed by As lattice,[69] with either Ca or K atoms or clusters scattered on top of it (Figs. 6(a) and 6(b)). Figure 6(c) shows comparison of dI/dV spectra at the vortex core (P1), middle (P2), edge (P3), and without the magnetic field (SC gap). A strong ZBP appears at the vortex core.

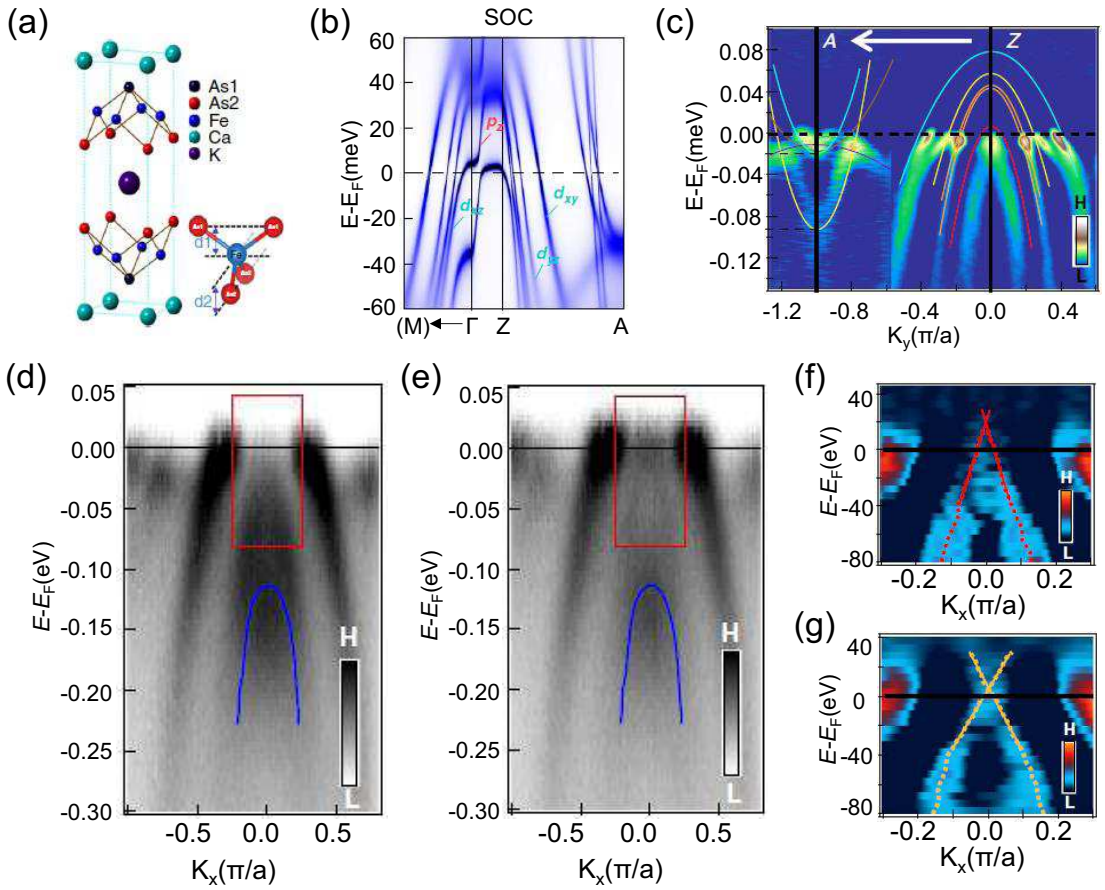

Fig. 5. Topological surface states in $CaKFe_4As_4$. (a) The crystal structure of $CaKFe_4As_4$. (b) DFT+DMFT calculation results for the band structures of $CaKFe_4As_4$ with SOC. (c) Second derivative of the ARPES intensity plot along the A–Z direction. (d) ARPES spectral intensity plots along the Γ–M direction on undoped $CaKFe_4As_4$. (e) Same as (d), but the sample is K doped. (f) and (g) The second-derivative plot of (d) and (e) within the red boxes, respectively.[43]

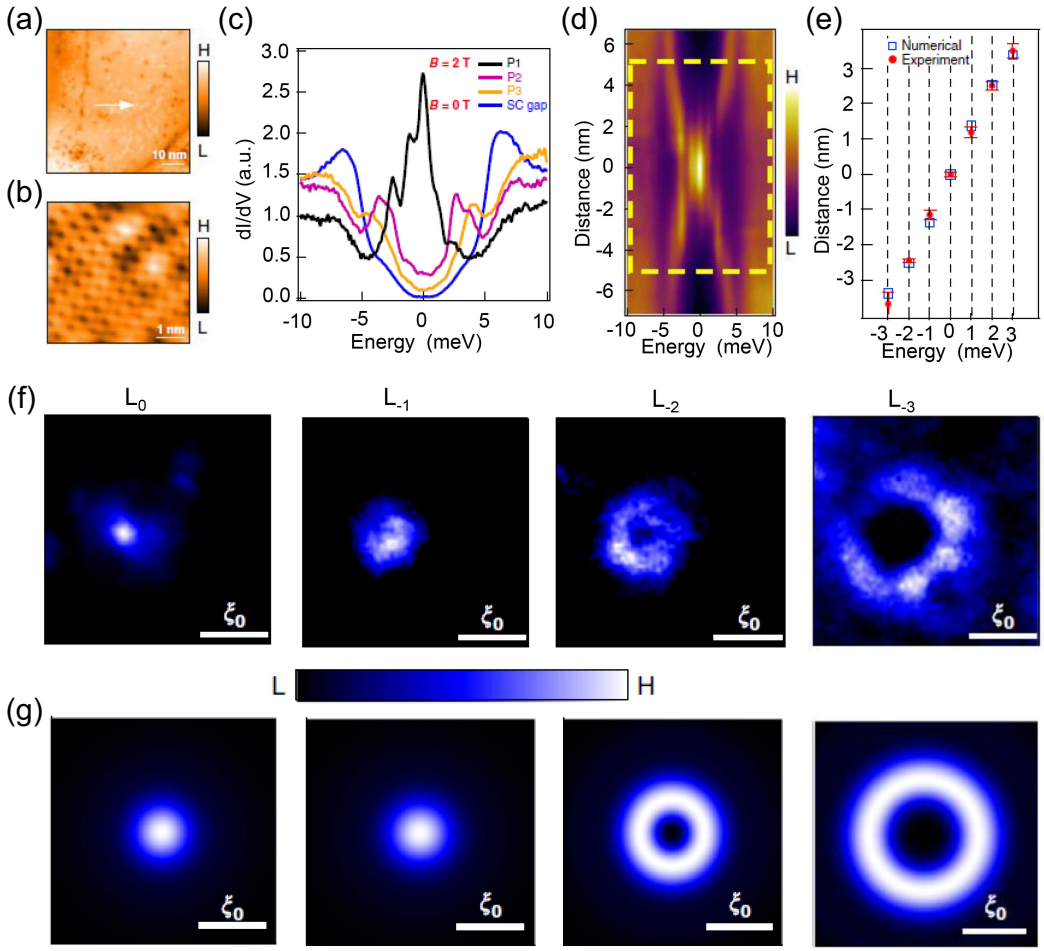

Fig. 6. MZM in a topological vortex core. (a) and (b) Large-scale (a) and atomically-resolved (b) STM topography of $CaKFe_4As_4$. (c) Comparison of dI/dV spectra at vortex core (P1), middle (P2), edge (P3), and without magnetic field (SC gap). (d) Intensity plot of dI/dV spectra detected across a topological vortex. (e) Comparison between the numerically calculated energy eigenvalues of CBSs and experimental values for different angular momenta. (f) Spatial patterns of vortex-bound states at bias voltages of 0 mV, −1.2 mV, −2.4 mV, and −3.6 mV, respectively. (g) Numerical calculations of the two-dimensional local density of L (MZM), L_{-1}, L_{-2}, and L_{-3}, respectively, which are based on the topological vortex core model.[43]

There is a hard SC gap at vortex core without magnetic field, which demonstrates that the ZBP is not induced by impurities. The intensity plot of a series spectra acquired cross vortex in Fig. 6(d) shows that the ZBP does not shift or split across the vortex. Besides the zero mode, there are several discrete in-gap bound states inside the vortex core. Similar to $FeTe_{0.55}Se_{0.45}$, the vortex core states marked by L_0, $L_{\pm1}$, $L_{\pm2}$, $L_{\pm3}$ also show a quantized sequence in Fig. 6(e). The model calculation with the same parameter set ($\Delta = 5.8$ meV, $E_F = 20.9$ meV, $\xi_0 = 6.4$ nm) reproduces the observed vortex core states (Fig. 6(e)).

The spatial distributions of the discrete bound states are obtained in dI/dV maps in Fig. 6(f). The MZM and the first level CBS (L_{-1}) show solid-circle pattern, while the other higher energy CBS (L_{-2} and L_{-3}) show hollow-ring patterns around the vortex. A general and direct numerical calculation based on the same parameters is carried out in Fig. 6(g), which agrees very well with the experimental results. The combined study by ARPES and STM/S shows a robust ZBP coexisting with higher-order CBSs with integer quantized energy level spacing, a strong evidence of the existence of MZM in $CaKFe_4As_4$. In addition, the higher superconducting transition temperature and more homogeneous bulk states make $CaKFe_4As_4$ as a practical platform for MZM research.

4. Impurity-assisted MZM in LiFeAs

As discussed above, the study of Fe(Te,Se) and $CaKFe_4As_4$ inspires people to look for the topological superconductors with homogeneous superconductivity at nanoscale and a non-polar cleaved surface. In iron pnictides, LiFeAs is a stoichiometric system with a SC transition temperature $T_c = 17$ K.[70,71] The mechanical cleavage happens between two Li layers (Fig. 7(a)), creating a non-polar cleaving surface.[72–76] Previous STM/S study demonstrated the homogeneous superconductivity on the LiFeAs surface.[73,75] Combined with the non-polar surface, LiFeAs is a promising platform to realize MZMs. Importantly, ARPES experiments showed the existence of two Dirac cone band structures around the Fermi level: a topological insulator (TI) Dirac cone at about −5 meV and a topological Dirac semimetal (TDS) Dirac cone at about +10 meV (Fig. 7(b)).[52] The mechanism of the topological band inversion in LiFeAs is very similar to that in Fe(Te,Se), which originates from the p band shifting downward and crossing with d bands. Thus, it is expected

that MZMs will emerge in the topological vortices. However, STM/S experiments show there is no ZBP in the vortex and only spatially dispersing CBSs exist,[72] which leaves a puzzle in this field.

To explore the MZM in LiFeAs, systematic STM/S experiments have been conducted. Kong *et al.* found that although the cleaved surface is non-polar, there are intrinsic impurities distributed across the surface.[44] As a result, after the magnetic field applied perpendicularly to the surface, some vortices appear at the impurity-free region (free vortices) while others appear as impurity-assisted vortices (Fig. 7(c)). For the free vortices, $\mathrm{d}I/\mathrm{d}V$ map shows that the vortex has a C_4 symmetry, which originates from the C_4 symmetry of the Fermi surface (Fig. 7(d)).[77] $\mathrm{d}I/\mathrm{d}V$ spectra line-cut across the free vortex shows only the dispersing CBSs as well as the discrete CBSs (Figs. 7(e) and 7(f)). Considering the SC gaps and the Fermi energy (E_F) of the d_{xy} and d_{yz} bands, it can be attributed that the dispersing CBSs come from the d_{xy} band while discrete CBSs come from the d_{yz} band.[44,78] It is should be noted that at every free vortex, no ZBP emerges. On the other hand, the impurity-assisted vortex presents an anisotropic structure owing to the influence of impurity (Figs. 8(a) and 8(b)).[79] The $\mathrm{d}I/\mathrm{d}V$ spectra line-cut across the impurity-assisted vortex shows that the ZBP emerges at the vortex center (Figs. 8(c) and 8(e)). The zero-field result excludes the possibility that the ZBP comes from impurity states (Fig. 8(d)).

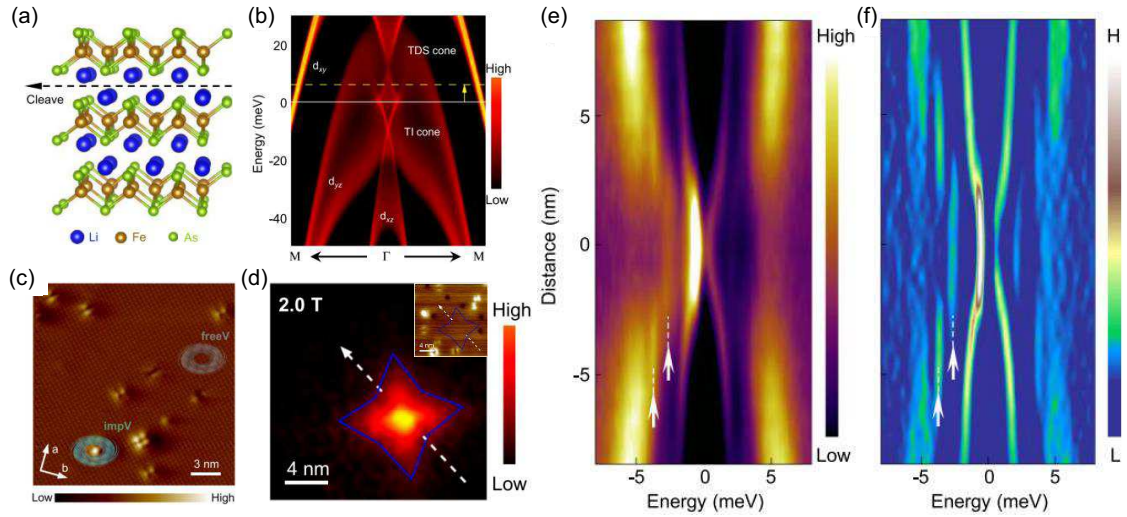

Fig. 7. Free vortex of LiFeAs. (a) The lattice structure of LiFeAs. The dashed arrow indicates where the cleavage happens. (b) The band structure near the Γ point adopted from the ARPES and DFT calculations results. (c) The atomic resolution of cleaved Li surface with impurities sporadically distributed. Vortices at impurity-free regions are called free vortices and those at impurity region are called impurity-assisted vortices. (d) The $\mathrm{d}I/\mathrm{d}V$ map of a free vortex at zero energy. Inset: the corresponding topography image. (e) The intensity plot of the $\mathrm{d}I/\mathrm{d}V$ spectra line-cut as indicated by the white dashed line in (d). (f) The curvature intensity plot of (e). White arrows in (e) and (f) indicate the discrete CBSs.[44]

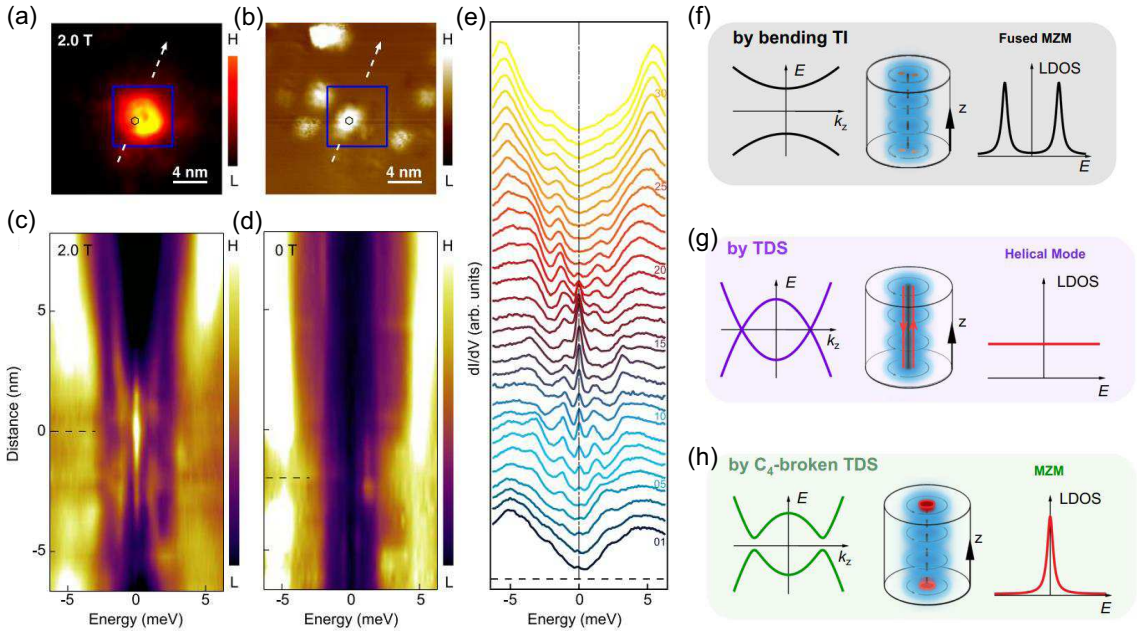

Fig. 8. Impurity-assisted vortex of LiFeAs. (a) Zero energy $\mathrm{d}I/\mathrm{d}V$ map of an impurity-assisted vortex. (b) The corresponding topography of (a). (c) The intensity plot of $\mathrm{d}I/\mathrm{d}V$ spectra line-cut across the impurity-assisted vortex as marked by the white dashed line in (a). (d) The same $\mathrm{d}I/\mathrm{d}V$ line-cut as (c) but at zero magnetic field. (e) The water-fall like plot of (c). (f)–(h) Sketches of the dispersion of lowest vortex bound states (left panel), the diagram of vortex line (middle panel), and the local density of states of Majorana mode (right panel) in the case of the bending topological insulator surface states (f), the topological Dirac semimetal with C_4 symmetry (g), and the topological Dirac semimetal with C_4 symmetry broken (h).[44]

Careful check at the ARPES results shows that the Fermi level crosses the TI topological surface twice,[52] inducing two MZMs in the same free vortex center. Hence, these two unprotested MZMs fuse with each to form Fermionic states locating on the two sides of the Fermi level (Fig. 8(f)). In the impurity-assisted vortex, impurities act as local electron doping centers, which shift the Fermi level upward towards the TDS region. This electron doping effect thus drives the system from TI phase to TDS phase (Fig. 8(g)).[80,81] In addition, the vortex structure suggests the local C_4 symmetry breaking, which can gap out the TDS Dirac cone with newly formed TSS in the gap. When the upshifted Fermi level crosses the new TSS, MZM can emerge at the vortex center (Fig. 8(h)). That is why MZMs only appear in the impurity-assisted vortices.

5. MZM without external magnetic field

All the above-mentioned cases need external magnetic field, which adds additional complexity in real application in the future. In addition, manipulating MZM is crucial for the braiding process, but moving vortices around each other is difficult. Therefore, realizing MZM in a novel system without necessity of applying external field will be of both fundamental and practical significance.

A robust ZBP was discovered on an interstitial iron atom residing on the surface of $FeTe_{0.55}Se_{0.45}$ without applying a magnetic field by Yin *et al.*[82] A theoretical work attributed the ZBP to MZM bound to a quantum anomalous vortex (QAV) nucleated spontaneously at the magnetic Fe atom.[83] The exchange coupling of the spin and orbital moment of the Fe impurity located at C_4 symmetric sites plays a similar role of the magnetic field. It generates circulating supercurrents by spin–orbital coupling and modulates the phase of the superconducting order parameter. Here, the C_4 symmetric site permits strong SOC. When the exchange coupling is strong enough, the Yu–Shiba–Rusinov (YSR) states will translate into MZM. This platform is suitable to manipulating and braiding MZM without applying magnetic field.

5.1. Reversible transition between YSR states and MZM by manipulating exchange coupling

Fan *et al.* deposited single iron atoms on the surface of $FeTe_{0.55}Se_{0.45}$ (Fig. 9(a)), and observed both YSR states and MZM on the Fe adatoms.[84] A series of dI/dV spectra detected across Fe adatom show a sharp ZBP with discrete bound states in Fig. 9(b). The peak positions of these bound states labeled by L_0, $L_{\pm1}$, $L_{\pm2}$ are acquired and displayed in Fig. 9(c). The energy positions follow an integer quantized sequence, which is identified as a topological hallmark of MZMs. In addition, the sharp ZBP does not shift or split under a high magnetic field up to 8 T, as shown in Fig. 9(d). This phenomenon is different from the topological-trivial YSR states or Kondo effect. All the observations provide strong evidence to the existence of MZM on the Fe adatom without applying magnetic field. We also note a recent work showing the absence of spin-polarization on a ZBP may be imaging the YSR states locating at a quantum phase transition point.[84,85]

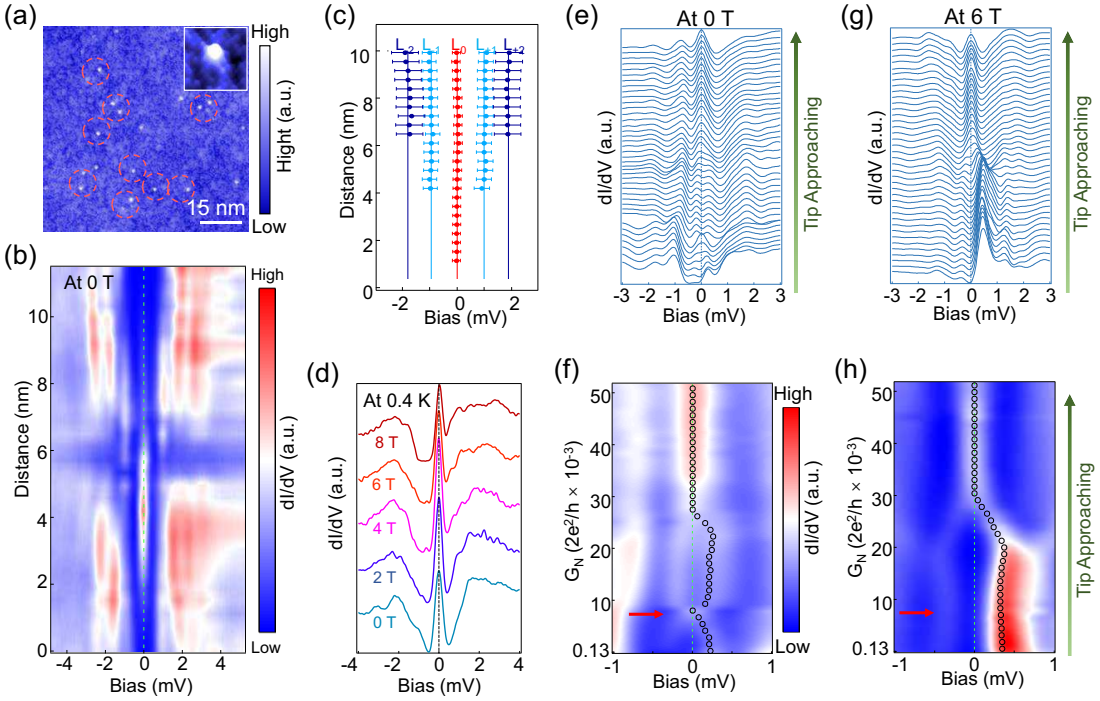

Fig. 9. Reversible transitions between YSR states and MZM by manipulating the exchange coupling. (a) STM image of $FeTe_{0.55}Se_{0.45}$ after monodispersed Fe atom deposition. (b) Intensity plot of a series of spectra detected across a Fe adatom. (c) The energies of the in-gap states at different spatial positions along the line-cut in (b). (d) Magnetic field dependence of the dI/dV spectra with a zero-bias peak. (e) and (f) Tunnel-barrier conductance dependence of the dI/dV spectra in (e) and its intensity plots in (f). (g) and (h) The same as (e) and (f), but measured under a magnetic field of 6 T.[84]

Intriguingly, the YSR states and MZM can be translated to each other by manipulating the exchange coupling between the adatom and the substrate. By approaching the STM tip from the top of the Fe adatom, the exchange coupling increases since the Fe adatoms are pushed towards the substrate. The tunnel-barrier conductance dependence of the $\mathrm{d}I/\mathrm{d}V$ spectra in Fig. 9(e) and its intensity plots in Fig. 9(f) are detected by approaching tip at 0 T. The two peaks of YSR states coalesce into a ZBP marked by the red arrow firstly and split again with approaching tip. With further approaching tip, the YSR states translate into robust ZBP which does not split finally. In order to explore the nature of the two ZBP during approaching tip, the same experiments were repeated at 6 T. The corresponding $\mathrm{d}I/\mathrm{d}V$ spectra and the intensity plots are displayed in Figs. 9(g) and 9(h). The first ZBP marked by the red arrow does not appear while the second robust ZBP appears again. In consideration of the high magnetic field, the first ZBP is the phase transition point of YSR states and splits at 6 T, while the second robust ZBP is MZM and keeps stable at high magnetic field.

5.2. Transition between YSR states and MZM by manipulating the adsorption site of Fe adatom

The transition between YSR states and MZM can also be induced by manipulating the adsorption site of Fe adatom, since the C_4 high symmetric site permits strongest SOC. First, the Fe adatom was moved away from the C_4 symmetric site by STM tip (Fig. 10(a)). The zero bias conductance map and the corresponding $\mathrm{d}I/\mathrm{d}V$ spectra across the Fe adatom are shown in Figs. 10(b) and 10(c), respectively. The ZBP disappears and YSR states appear. Then the Fe adatom was moved back to the original C_4 symmetric site (Fig. 10(d)). The zero bias conductance map changes in Fig. 10(e) and the ZBP appears again in Fig. 10(f). The Fe adatom was then removed, as shown in Fig. 10(g). The zero bias conductance map shows no pattern in Fig. 10(h) and the hard SC gap recovers in Fig. 10(i), which indicates that the bound states are induced by the Fe adatom.

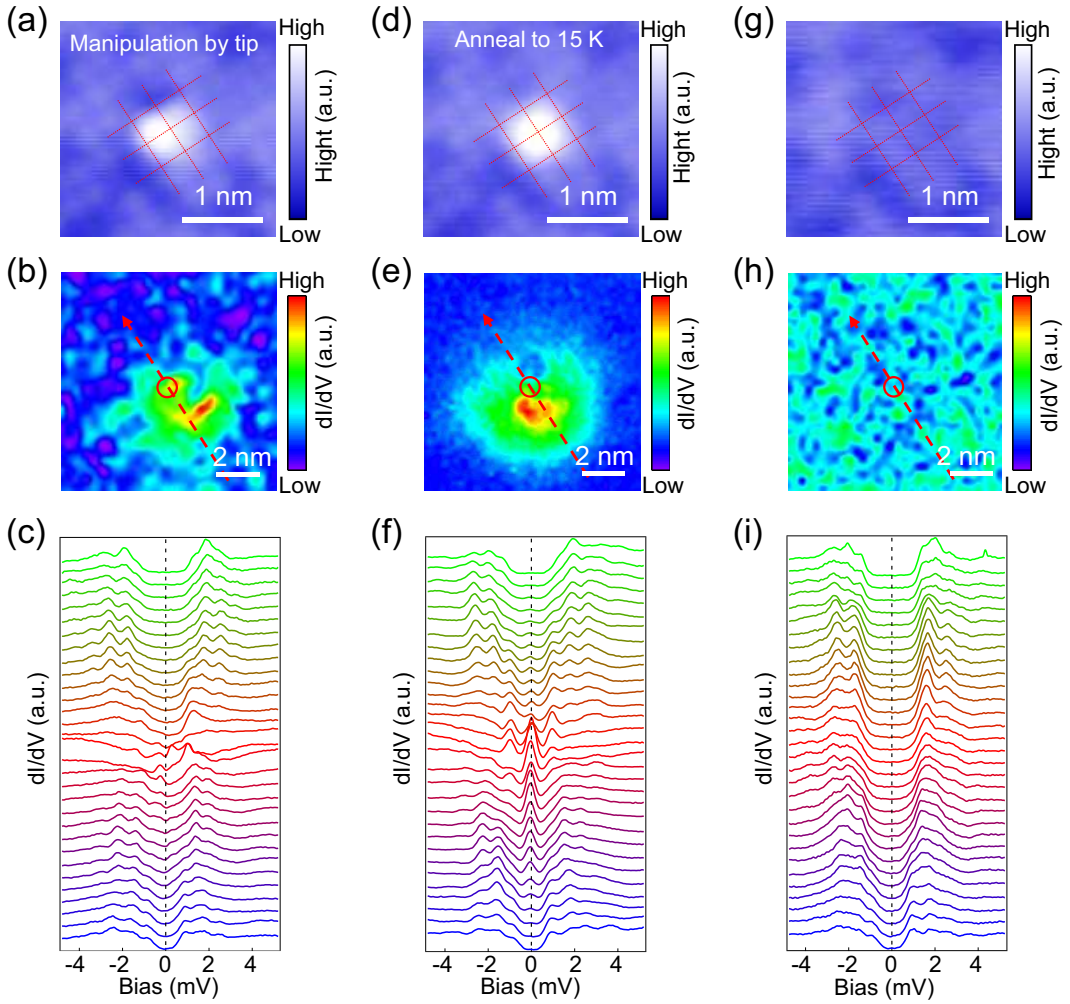

Fig. 10. Transitions between YSR states and MZM by manipulating the adsorption site of a Fe adatom. (a) STM image showing that the Fe adatom has been moved off the C_4 symmetric site by the tip. (b) Zero-energy $\mathrm{d}I/\mathrm{d}V$ map in the same region of (a). (c) $\mathrm{d}I/\mathrm{d}V$ line-cut spectra along the red dashed arrow in (b). (d) STM image showing that the Fe adatom moves back to the center of four Te adatoms. (e) Zero-energy $\mathrm{d}I/\mathrm{d}V$ map in the same region of (d). (f) $\mathrm{d}I/\mathrm{d}V$ line-cut spectra along the red dashed arrow in (e). (g) STM image showing that the Fe adatom is moved away. (h) Zero-energy $\mathrm{d}I/\mathrm{d}V$ map in the same region of (g). (i) $\mathrm{d}I/\mathrm{d}V$ line-cut spectra along the red dashed arrow in (h).[84]

6. Tunning the topological band structures by uniaxial strain

The impurity-assisted vortex in LiFeAs as well as the QAV state induced by Fe adatom in Fe(Te,Se) underscore that tuning the topological band structures of IBSs is a promising strategy to create robust MZMs. Among these Fe-based topological superconductors discussed above, LiFeAs is unique since it has nano-scale homogeneity and no other intervened orders.[70,73,75] Cao *et al.* found that on certain regions of the the cleaved surface of LiFeAs, 1D wrinkle structures manifesting as hump features can be found (Fig. 11(a)).[86] It is common that the change in topography will induce local strains which can tune the local band structures.[87,88]

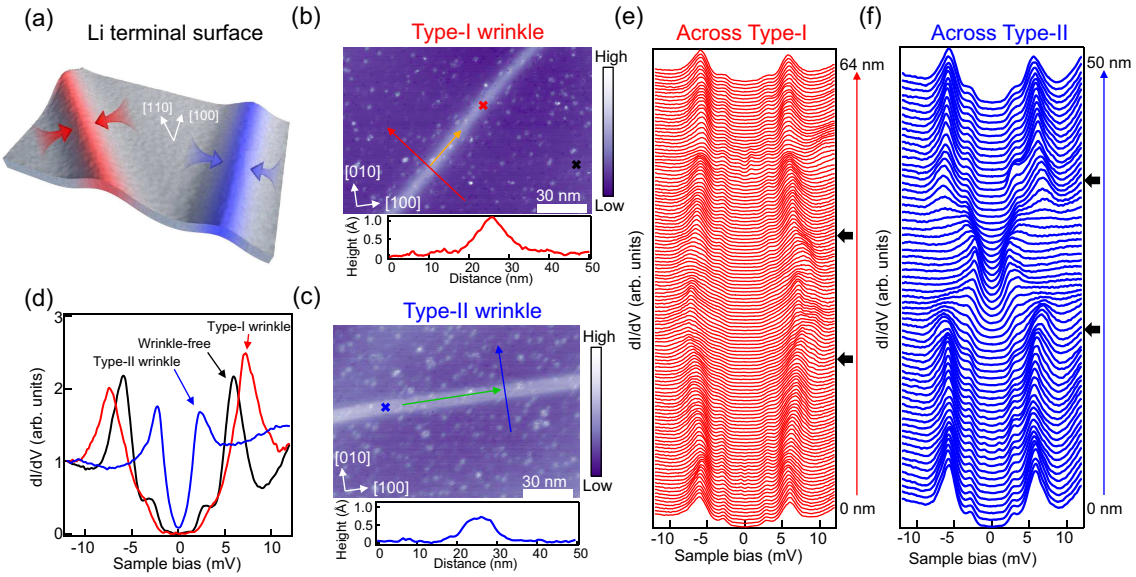

Fig. 11. Superconductivity of wrinkles on LiFeAs. (a) Schematic of the two types of wrinkles on LiFeAs surface. (b) The STM topography of type-I wrinkle and the corresponding line-profile. (c) The STM topography of type-II wrinkle and the corresponding line-profile. (d) The $\mathrm{d}I/\mathrm{d}V$ spectra at the wrinkle-free region (black), the type-I wrinkle region (red), and the type-II wrinkle region (blue). (e) The $\mathrm{d}I/\mathrm{d}V$ spectra line-cut across the type-I wrinkle as marked by the red arrow in (b). (f) The $\mathrm{d}I/\mathrm{d}V$ spectra line-cut across the type-II wrinkle as marked by the blue arrow in (c).[86]

The wrinkles on the surface fall into two categories (Figs. 11(b) and 11(c)). Typical type-I wrinkle is along the [110] direction (Fe–Fe direction) while typical type-II wrinkle is along the [100] direction (Fe–As direction). The major difference between these two types of wrinkles is their effects on SC gap sizes (Fig. 11(d)). At the wrinkle-free region, two SC gaps are detected. The large SC gap has a size of ~ 5.8 meV and the small SC gap has a size of ~ 2.9 meV. Compared with the results from ARPES,[52] it can be conclude that the 5.8 meV gap comes from d_{yz} band and the 2.9 meV gap comes from d_{xy} band. Surprisingly, at the type-I wrinkle, both SC gap sizes are enhanced. The large SC gap has a size of 7.3 meV and the small SC gap has a size of 3.6 meV. However, at the type-II wrinkle, the large SC gap is totally suppressed and only a 2.5 meV gap is seen. The $\mathrm{d}I/\mathrm{d}V$ spectra line-cut across two types of wrinkles show that the SC gaps change at the edges of the wrinkles (Figs. 11(e) and 11(f)), indicating that the superconductivity is strongly influenced by the wrinkles.

The vortex at the wrinkle-free region shows a C_4 symmetry (Fig. 12(a)), while that at the wrinkled regions shows a C_2 symmetry (Fig. 12(b)). This contrast suggests the existence of local strain and the Fermi surface has changed. By statistics, it is found that type-I wrinkle favors the [110] direction and type-II wrinkle favors the [100] direction (Fig. 12(c)). The gap size versus the orientation of wrinkle shows an abrupt change. Local strain affects not only the SC gap sizes but also the local density of states above the Fermi level. The shoulder at about $+33$ meV is assigned to the d_{xy} band top.[89] This shoulder shifts to high energy at type-I region and shifts to low energy at type-II region, indicating the shift of the d_{xy} band top (Fig. 12(d)). Based on the experimental results, a possible scenario is proposed that local strain causes the band shifting around the Γ point (Figs. 12(e)–12(g)). On the type-I wrinkle, the d_{xz} band shifts upward and crosses the Fermi level, resulting in the enhancement of density of states and increasing of SC gaps. On the type-II wrinkle, the d_{xz} and d_{yz} bands shift downward and only the d_{xy} band crosses the Fermi level. The d_{xy} band has a small gap which is consistent with the small gap in the $\mathrm{d}I/\mathrm{d}V$ spectra.

Observations on wrinkles indicate that the uniaxial strain has two effects on LiFeAs. First, the uniaxial strain can shift the Fermi level upward. Second, the uniaxial strain breaks the local C_4 symmetry. These two effects are exactly the requirement for tuning MZM in LiFeAs as discussed in Section 4. Therefore, utilizing the strain effect to tune the MZM is a promising strategy in the future.[90–93]

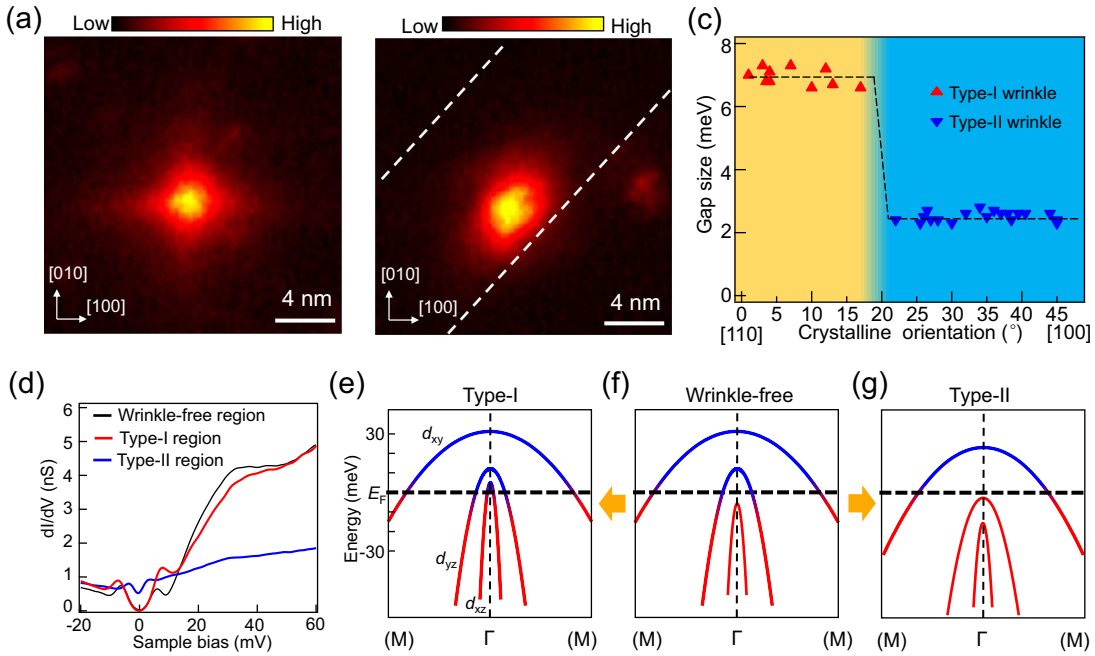

Fig. 12. Local band structures of wrinkles on LiFeAs. (a) and (b) The zero-bias conductance map of vortices at wrinkle-free and type-I wrinkle, respectively. (c) The statistics of the gap sizes versus the wrinkle orientations. The dashed line is a guide to eye. (d) Wide-range $\mathrm{d}I/\mathrm{d}V$ spectra at the wrinkle-free (black), type-I wrinkle (red), and type-II wrinkle (blue). (e)–(g) The sketches of the band structures of LiFeAs near the Γ point, showing the band shifting effect from the wrinkles.[86]

7. Conclusion and outlook

In this topical review, we present an overview of the STM studies on MZMs in IBSs. The $FeTe_{0.55}Se_{0.45}$ system offers the first platform in IBSs supporting MZM. However, the intrinsic inhomogeneity of $FeTe_{0.55}Se_{0.45}$ sets obstacle to its real application. Another candidate of the iron-chalcogenides, $(Li_{0.84}Fe_{0.16})OHFeSe$, suffers from the same issue due to the chemical doping. $CaKFe_4As_4$ has a more homogeneous bulk state compared with $FeTe_{0.55}Se_{0.45}$, but its cleaving surface is polar and the Ca and K atoms are randomly distributed on top, giving rise to different chemical potentials across the surface. LiFeAs has a non-polar cleaving surface and homogeneous bulk states. However, the complicated bulk and surface band structures near the Fermi level lead to the absence of MZM in the free vortices.

Combining all these information together, it seems that exploring the ideal platform in IBSs for MZM research is challenging but necessary. Several issues, such as the disordered vortex distribution, low yield of topological vortices, high sensitivity of the MZM to the local environment change, and lack of practical protocol to control the vortices, are still holding back the goal of braiding MZMs. An alternative way might be focusing on the existing platforms and trying to engineer their band structures and physical properties, as has been elaborated in Sections 5 and 6. Both routes are difficult, and the theorists, experimentalists and materialists have to work together to make it happen.

Acknowledgements

The work is supported by the Ministry of Science and Technology of China (Grant No. 2019YFA0308500) and the Chinese Academy of Sciences (Grant Nos. XDB28000000 and YSBR-003).

References

[1] Majorana E 1937 *Nuovo Ciment* **14** 171
[2] Alicea J 2012 *Rep. Prog. Phys.* **75** 076501
[3] Qi X L and Zhang S C 2011 *Rev. Mod. Phys.* **83** 1057
[4] Wilczek F 2009 *Nat. Phys.* **5** 614
[5] Kitaev A Y 2003 *Ann. Phys-new. York.* **303** 2
[6] Beenakker C W J 2013 *Annu. Rev. Condens. Matter Phys.* **4** 113
[7] Nayak C, Simon S H, Stern A, Freedman M and Das Sarma S 2008 *Rev. Mod. Phys.* **80** 1083
[8] Aasen D, Hell M, Mishmash R V, Higginbotham A, Danon J, Leijnse M, Jespersen T S, Folk J A, Marcus C M, Flensberg K and Alicea J 2016 *Phys. Rev. X* **6** 031016
[9] Fu L and Kane C L 2008 *Phys. Rev. Lett.* **100** 096407
[10] Read N and Green D 2000 *Phys. Rev. B* **61** 10267
[11] Ivanov D A 2001 *Phys. Rev. Lett.* **86** 268
[12] Kitaev A Y 2001 *Phys. Uspekhi* **44** 131
[13] Lutchyn R M, Sau J D and Das Sarma S 2010 *Phys. Rev. Lett.* **105** 077001
[14] Sau J D, Lutchyn R M, Tewari S and Das Sarma S 2010 *Phys. Rev. Lett.* **104** 040502
[15] Braunecker B and Simon P 2013 *Phys. Rev. Lett.* **111** 147202
[16] Klinovaja J, Stano P, Yazdani A and Loss D 2013 *Phys. Rev. Lett.* **111** 186805
[17] Nadj-Perge S, Drozdov I K, Bernevig B A and Yazdani A 2013 *Phys. Rev. B* **88** 020407
[18] Vazifeh M M and Franz M 2013 *Phys. Rev. Lett.* **111** 206802
[19] Li J, Neupert T, Wang Z J, MacDonald A H, Yazdani A and Bernevig B A 2016 *Nat. Commun.* **7** 12297
[20] Mourik V, Zuo K, Frolov S M, Plissard S R, Bakkers E P A M and Kouwenhoven L P 2012 *Science* **336** 1003

[21] Deng M T, Yu C L, Huang G Y, Larsson M, Caroff P and Xu H Q 2012 *Nano Lett.* **12** 6414

[22] Churchill H O H, Fatemi V, Grove-Rasmussen K, Deng M T, Caroff P, Xu H Q and Marcus C M 2013 *Phys. Rev. B* **87** 241401

[23] Deng M T, Vaitiekenas S, Hansen E B, Danon J, Leijnse M, Flensberg K, Nygard J, Krogstrup P and Marcus C M 2016 *Science* **354** 1557

[24] Lutchyn R M, Bakkers E P A M, Kouwenhoven L P, Krogstrup P, Marcus C M and Oreg Y 2018 *Nat. Rev. Mater.* **3** 52

[25] Nadj-Perge S, Drozdov I K, Li J, Chen H, Jeon S, Seo J, MacDonald A H, Bernevig B A and Yazdani A 2014 *Science* **346** 602

[26] Ruby M, Pientka F, Peng Y, von Oppen F, Heinrich B W and Franke K J 2015 *Phys. Rev. Lett.* **115** 197204

[27] Ruby M, Heinrich B W, Peng Y, von Oppen F and Franke K J 2017 *Nano Lett.* **17** 4473

[28] Kim H, Palacio-Morales A, Posske T, Rozsa L, Palotas K, Szunyogh L, Thorwart M and Wiesendanger R 2018 *Sci. Adv.* **4** eaar5251

[29] Schneider L, Beck P, Posske T, Crawford D, Mascot E, Rachel S, Wiesendanger R and Wiebe J 2021 *Nat. Phys.* **17** 943

[30] Schneider L, Beck P, Neuhaus-Steinmetz J, Rozsa L, Posske T, Wiebe J and Wiesendanger R 2022 *Nat. Nanotechnol.* **17** 384

[31] Palacio-Morales A, Mascot E, Cocklin S, Kim H, Rachel S, Morr D K and Wiesendanger R 2019 *Sci. Adv.* **5** eaav6600

[32] Kezilebieke S, Huda M N, Vano V, Aapro M, Ganguli S C, Silveira O J, Glodzik S, Foster A S, Ojanen T and Liljeroth P 2020 *Nature* **588** 424

[33] Kezilebieke S, Silveira O J, Huda M N, Vano V, Aapro M, Ganguli S C, Lahtinen J, Mansell R, van Dijken S, Foster A S and Liljeroth P 2021 *Adv. Mater.* **33** 2006850

[34] Nayak A K, Steinbok A, Roet Y, Koo J, Margalit G, Feldman I, Almoalem A, Kanigel A, Fiete G A, Yan B H, Oreg Y, Avraham N and Beidenkopf H 2021 *Nat. Phys.* **17** 1413

[35] Kezilebieke S, Vano V, Huda M N, Aapro M, Ganguli S C, Liljeroth P and Lado J L 2022 *Nano Lett.* **22** 328

[36] Xu J P, Wang M X, Liu Z L, Ge J F, Yang X, Liu C, Xu Z A, Guan D, Gao C L, Qian D, Liu Y, Wang Q H, Zhang F C, Xue Q K and Jia J F 2015 *Phys. Rev. Lett.* **114** 017001

[37] Sun H H, Zhang K W, Hu L H, Li C, Wang G Y, Ma H Y, Xu Z A, Gao C L, Guan D D, Li Y Y, Liu C, Qian D, Zhou Y, Fu L, Li S C, Zhang F C and Jia J F 2016 *Phys. Rev. Lett.* **116** 257003

[38] Zhang P, Yaji K, Hashimoto T, Ota Y, Kondo T, Okazaki K, Wang Z, Wen J, Gu G D, Ding H and Shin S 2018 *Science* **360** 182

[39] Wang D, Kong L, Fan P, Chen H, Zhu S, Liu W, Cao L, Sun Y, Du S, Schneeloch J, Zhong R, Gu G, Fu L, Ding H and Gao H J 2018 *Science* **362** 333

[40] Li G, Zhu S Y, Wang D F, Wang Y L and Gao H J 2021 *Supercond. Sci. Tech.* **34** 073001

[41] Fernandes R M, Coldea A I, Ding H, Fisher I R, Hirschfeld P J and Kotliar G 2022 *Nature* **601** 35

[42] Liu Q, Chen C, Zhang T, Peng R, Yan Y J, Wen C H P, Lou X, Huang Y L, Tian J P, Dong X L, Wang G W, Bao W C, Wang Q H, Yin Z P, Zhao Z X and Feng D L 2018 *Phys. Rev. X* **8** 041056

[43] Liu W Y, Cao L, Zhu S Y, Kong L Y, Wang G W, Papaj M, Zhang P, Liu Y B, Chen H, Li G, Yang F Z, Kondo T, Du S X, Cao G H, Shin S, Fu L, Yin Z P, Gao H J and Ding H 2020 *Nat. Commun.* **11** 5688

[44] Kong L Y, Cao L, Zhu S Y, Papaj M, Dai G Y, Li G, Fan P, Liu W Y, Yang F Z, Wang X C, Du S X, Jin C Q, Fu L, Gao H J and Ding H 2021 *Nat. Commun.* **12** 4146

[45] Zhu S, Kong L, Cao L, Chen H, Papaj M, Du S, Xing Y, Liu W, Wang D, Shen C, Yang F, Schneeloch J, Zhong R, Gu G, Fu L, Zhang Y Y, Ding H and Gao H J 2020 *Science* **367** 189

[46] Wang Z Y, Rodriguez J O, Jiao L, Howard S, Graham M, Gu G D, Hughes T L, Morr D K and Madhavan V 2020 *Science* **367** 104

[47] Chen C, Jiang K, Zhang Y, Liu C F, Liu Y, Wang Z Q and Wang J 2020 *Nat. Phys.* **16** 536

[48] Machida T, Sun Y, Pyon S, Takeda S, Kohsaka Y, Hanaguri T, Sasagawa T and Tamegai T 2019 *Nat. Mater.* **18** 811

[49] Caroli C, De Gennes P G and Matricon J 1964 *Phys. Lett.* **9** 307

[50] Hess H F, Robinson R B and Waszczak J V 1990 *Phys. Rev. Lett.* **64** 2711

[51] Zhang P, Richard P, Xu N, Xu Y M, Ma J, Qian T, Fedorov A V, Denlinger J D, Gu G D and Ding H 2014 *Appl. Phys. Lett.* **105** 172601

[52] Zhang P, Wang Z J, Wu X X, Yaji K, Ishida Y, Kohama Y, Dai G Y, Sun Y, Bareille C, Kuroda K, Kondo T, Okazaki K, Kindo K, Wang X C, Jin C Q, Hu J P, Thomale R, Sumida K, Wu S L, Miyamoto K, Okuda T, Ding H, Gu G D, Tamegai T, Kawakami T, Sato M and Shin S 2019 *Nat. Phys.* **15** 41

[53] Wang Z J, Zhang P, Xu G, Zeng L K, Miao H, Xu X Y, Qian T, Weng H M, Richard P, Fedorov A V, Ding H, Dai X and Fang Z 2015 *Phys. Rev. B* **92** 115119

[54] Xu G, Lian B, Tang P Z, Qi X L and Zhang S C 2016 *Phys. Rev. Lett.* **117** 047001

[55] Chiu C K, Machida T, Huang Y Y, Hanaguri T and Zhang F C 2020 *Sci. Adv.* **6** eaay0443

[56] Kong L, Zhu S, Papaj M, Chen H, Cao L, Isobe H, Xing Y, Liu W, Wang D, Fan P, Sun Y, Du S, Schneeloch J, Zhong R, Gu G, Fu L, Gao H J and Ding H 2019 *Nat. Phys.* **15** 1181

[57] Liu C X, Sau J D, Stanescu T D and Das Sarma S 2017 *Phys. Rev. B* **96** 075161

[58] Moore C, Stanescu T D and Tewari S 2018 *Phys. Rev. B* **97** 165302

[59] Moore C, Zeng C C, Stanescu T D and Tewari S 2018 *Phys. Rev. B* **98** 155314

[60] Flensberg K 2010 *Phys. Rev. B* **82** 180516

[61] Setiawan F, Liu C X, Sau J D and Das Sarma S 2017 *Phys. Rev. B* **96** 184520

[62] Law K T, Lee P A and Ng T K 2009 *Phys. Rev. Lett.* **103** 237001

[63] Wimmer M, Akhmerov A R, Dahlhaus J P and Beenakker C W J 2011 *New J. Phys.* **13** 053016

[64] Sau J 2020 *Science* **367** 145

[65] Sau J, Simon S, Vishveshwara S and Williams J R 2020 *Nature Reviews Physics* **2** 667

[66] He X, Li G, Zhang J, Karki A B, Jin R, Sales B C, Sefat A S, McGuire M A, Mandrus D and Plummer E W 2011 *Phys. Rev. B* **83** 220502

[67] Iyo A, Kawashima K, Kinjo T, Nishio T, Ishida S, Fujihisa H, Gotoh Y, Kihou K, Eisaki H and Yoshida Y 2016 *J. Am. Chem. Soc.* **138** 3410

[68] Meier W R, Kong T, Bud'ko S L and Canfield P C 2017 *Phys. Rev. Materials* **1** 013401

[69] Gao M A, Ma F J, Lu Z Y and Xiang T 2010 *Phys. Rev. B* **81** 193409

[70] Wang X C, Zhang S J, Liu Q Q, Deng Z, Lv Y X, Zhu J L, Feng S M and Jin C Q 2011 *High Pressure Res.* **31** 7

[71] Wang X C, Liu Q Q, Lv Y X, Gao W B, Yang L X, Yu R C, Li F Y and Jin C Q 2008 *Solid State Commun.* **148** 538

[72] Hanaguri T, Kitagawa K, Matsubayashi K, Mazaki Y, Uwatoko Y and Takagi H 2012 *Phys. Rev. B* **85** 214505

[73] Chi S, Grothe S, Liang R X, Dosanjh P, Hardy W N, Burke S A, Bonn D A and Pennec Y 2012 *Phys. Rev. Lett.* **109** 087002

[74] Allan M P, Rost A W, Mackenzie A P, Xie Y, Davis J C, Kihou K, Lee C H, Iyo A, Eisaki H and Chuang T M 2012 *Science* **336** 563

[75] Yin J X, Zhang S S, Dai G Y, Zhao Y Y, Kreisel A, Macam G, Wu X X, Miao H, Huang Z Q, Martiny J H J, Andersen B M, Shumiya N, Multer D, Litskevich M, Cheng Z J, Yang X, Cochran T A, Chang G Q, Belopolski I, Xing L Y, Wang X C, Gao Y, Chuang F C, Lin H, Wang Z Q, Jin C Q, Bang Y and Hasan M Z 2019 *Phys. Rev. Lett.* **123** 217004

[76] Yim C M, Trainer C, Aluru R, Chi S, Hardy W N, Liang R X, Bonn D and Wahl P 2018 *Nat. Commun.* **9** 2602

[77] Wang Y, Hirschfeld P J and Vekhter I 2012 *Phys. Rev. B* **85** 020506

[78] Umezawa K, Li Y, Miao H, Nakayama K, Liu Z H, Richard P, Sato T, He J B, Wang D M, Chen G F, Ding H, Takahashi T and Wang S C 2012 *Phys. Rev. Lett.* **108** 037002

[79] Balatsky A V, Vekhter I and Zhu J X 2006 *Rev. Mod. Phys.* **78** 373

[80] Konig E J and Coleman P 2019 *Phys. Rev. Lett.* **122** 207001

[81] Qin S S, Hu L H, Le C C, Zeng J F, Zhang F C, Fang C and Hu J P 2019 *Phys. Rev. Lett.* **123** 027003

[82] Yin J X, Wu Z, Wang J H, Ye Z Y, Gong J, Hou X Y, Shan L, Li A, Liang X J, Wu X X, Li J, Ting C S, Wang Z Q, Hu J P, Hor P H, Ding H and Pan S H 2015 *Nat. Phys.* **11** 543

[83] Jiang K, Dai X and Wang Z Q 2019 *Phys. Rev. X* **9** 011033

[84] Fan P, Yang F Z, Qian G J, Chen H, Zhang Y Y, Li G, Huang Z H, Xing Y Q, Kong L Y, Liu W Y, Jiang K, Shen C M, Du S X, Schneeloch J, Zhong R D, Gu G D, Wang Z Q, Ding H and Gao H J 2021 *Nat. Commun.* **12** 1348

[85] Wang D, Wiebe J, Zhong R, Gu G and Wiesendanger R 2021 *Phys. Rev. Lett.* **126** 076802

[86] Cao L, Liu W Y, Li G, Dai G Y, Zheng Q, Wang Y X, Jiang K, Zhu S Y, Huang L, Kong L Y, Yang F Z, Wang X C, Zhou W, Lin X, Hu J P, Jin C Q, Ding H and Gao H J 2021 *Nat. Commun.* **12** 6312

[87] Edelberg D, Kumar H, Shenoy V, Ochoa H and Pasupathy A N 2020 *Nat. Phys.* **16** 1097
[88] Mao J H, Milovanovic S P, Andelkovic M, Lai X Y, Cao Y, Watanabe K, Taniguchi T, Covaci L, Peeters F M, Geim A K, Jiang Y H and Andrei E Y 2020 *Nature* **584** 215
[89] Miao H, Wang L M, Richard P, Wu S F, Ma J, Qian T, Xing L Y, Wang X C, Jin C Q, Chou C P, Wang Z, Ku W and Ding H 2014 *Phys. Rev. B* **89** 220503
[90] Sau J D, Clarke D J and Tewari S 2011 *Phys. Rev. B* **84** 094505
[91] van Heck B, Akhmerov A R, Hassler F, Burrello M and Beenakker C W J 2012 *New J. Phys.* **14** 035019
[92] Vijay S and Fu L 2016 *Phys. Rev. B* **94** 235446
[93] Karzig T, Knapp C, Lutchyn R M, Bonderson P, Hastings M B, Nayak C, Alicea J, Flensberg K, Plugge S, Oreg Y, Marcus C M and Freedman M H 2017 *Phys. Rev. B* **95** 235305